Cu 3 Te 2 O 5 (OH) 4 : a frustrated 2D quantum "magnetic raft" as a possible pathway to a spin liquid

Tianyu Zhu, Bei Zhu, Olivier Mentré, Suheon Lee, Dan Chen, Yanling Jin, Wenxuan Zhu, Ángel Arévalo-López, Claire Minaud, Kwang-Yong Choi, et al.

$Cu_3Te_2O_5(OH)_4$: a frustrated 2D quantum "*magnetic raft*" as a possible pathway to a spin liquid

Tianyu Zhu,[a,*] Bei Zhu,[a,*] Olivier Mentré,[b,#] Suheon Lee,[c] Dan Chen,[d] Yanling Jin,[d] Wenxuan Zhu,[d] Ángel M. Arévalo-López,[b] Claire Minaud,[e] Kwang-Yong Choi,[f] Minfeng Lü,[a,#]

[a]*School of Materials Science and Engineering, Jiangsu University of Science and Technology, Zhenjiang 212003, Jiangsu, China*

[b]*Université Lille Nord de France, UMR 8181 CNRS, Unité de Catalyse et de Chimie du Solide (UCCS USTL), F-59655 Villeneuve d'Ascq, France.*

[c]*Center for Integrated Nanostructure Physics, Institute for Basic Science (IBS), Suwon 16419, Republic of Korea*

[d]*School of Environmental & Chemical Engineering, Jiangsu University of Science and Technology, Zhenjiang 212003, Jiangsu, Perople's Republic of China*

[e]*Univ. Lille, CNRS, INRAE, Centrale Lille, Univ. Artois, FR 2638 - IMEC - Institut Michel-Eugène Chevreul, F-59000 Lille, France*

[f]*Department of Physics, Sungkyunkwan University, Suwon 16419, Republic of Korea*

*These authors contributed equally to this work.

Highlight:

$Cu_3Te_2O_5(OH)_4$ reveals a novel magnetic topology "*magnetic raft*" with frustrated tetrahedral knots, which may provide an unprecedented platform for discovering sought-after quantum spin liquids.

TOC graphic
“For Table of Contents Only”

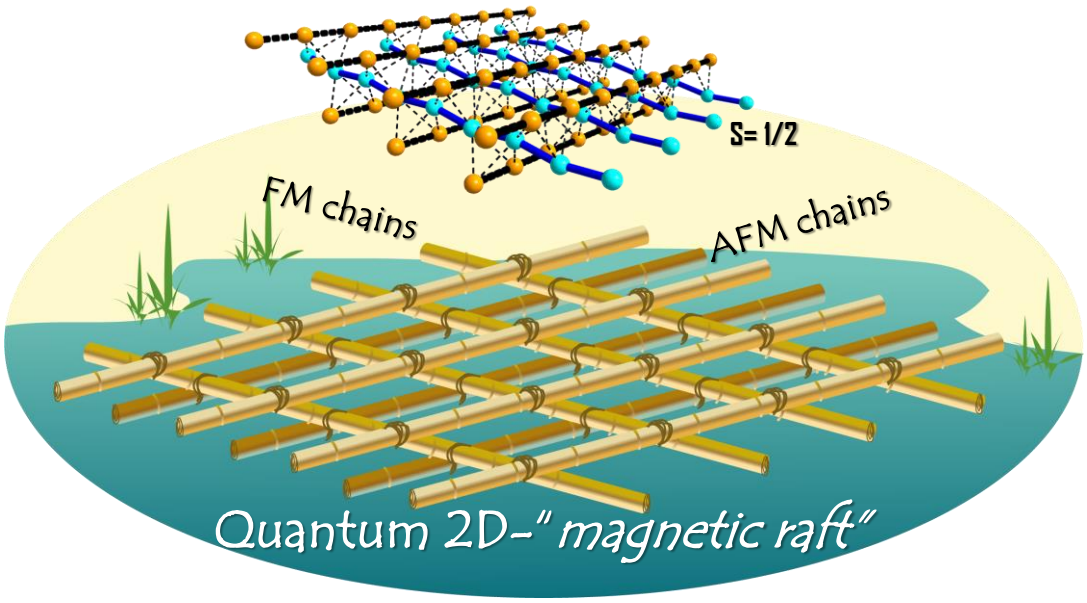

Abstract

We report a combined experimental and theoretical study of the hitherto unknown compound $Cu_3Te_2O_5(OH)_4$ that comprises an original network of ferromagnetic (FM, J_1 = -100 K with strong next-nearest neighbors exchanges J_{NNN} = 50 K) chains and alternating antiferromagnetic (AFM, J_2 ~148 K, $J_{2'}$ ~125 K) chains arranged in a so-called S=1/2 two-dimensional (2D) "*magnetic raft*" spin lattice. The two 1D spin sub-lattices are interconnected by weaker exchanges (J_d ~40 K), which create tetrahedral Cu_4 knots between the cross-linked "*raft"* legs, bringing about strong magnetic frustration. The magnetic susceptibility and specific heat show the absence of magnetic ordering down to 1.8 K hampered by fully frustrated Cu1 spins. High-field magnetization reveals a 1/3rd magnetization plateau stable as high as 33 T, which conveys the fingerprint of the individual AFM and FM chains. Magnetic entropy shows a two-stage Schottky-like release, implying the thermal decoupling of magnetic sublattices. Our work establishes that $Cu_3Te_2O_5(OH)_4$ can serve as a prominent platform for discovering sought-after quantum spin liquids in chemistry and physics.

Keywords : "*Magnetic raft*", low-dimensionality, frustration, quantum spin liquid

1. Introduction

Magnetic frustration and lattice dimensionality are two key ingredients that harbor exotic phenomena and unconventional states of matter, such as heavy fermion behavior,[1] quantum spin liquids (QSLs),[2] spin ice,[3] superconductivity,[4,5] and topological states.[6-8] In one or two spatial dimensions, the Mermin-Wagner theorem states that long-range ordering does not occur at finite temperatures in systems with sufficiently short-range isotropic interactions and without magneto-crystalline anisotropy.[9] This aspect has been extensively studied and well understood in weakly coupled spin chains.[10-11]Irrespective of whether interchain coupling is frustrated or unfrustrated, the Tomonaga-Luttinger liquid is fragile against long-range fluctuations

when isolated spin chains are coupled via interchain couplings. Actually, it poses a great challenge in achieving liquid-like ground states as the spatial dimensionality is increased above one-dimensional systems. As such, it deserves for chemists to discover suitable candidate materials.

In 2D systems, one of the most representative frustrated systems is the Kagomé lattice that is a corner-sharing network of triangles, as found in $[NH_4]_2[C_7H_{14}N][V_7O_6F_{18}]$[12]and $ZnCu_3(OH)_6Cl_2$.[13] Recently, structural derivatives related to the Kagomélattices (2D frustrated systems) including a star lattice (triangle-dodecagon), [14] capped-Kagomé network,[15] and diluted Kagomé lattice[16] have been developed by chemists.

In 1D systems, also the main theme is to achieve QSL ground states. The suppression of long-range magnetic order is pronounced due to enhanced quantum fluctuations,[9] as exemplified in $CuSiO_3$,[17] $BaCu_2Si_2O_7$,[18] and $BaCu_2Ge_2O_7$,[19] while $CuGeO_3$ showed a spin-Peierls transition at low temperature, leading to the opening of an energy gap.[20] However, there have been few reported strategies for low-dimensional frustrated magnets based on more complex arrangements,[21] and not much attention has been given to emergent magnetism when heterogeneous low-dimensional sub-units with different types of exchange interactions and spin topology are interconnected. In case local spin constraints are imposed to promote quantum fluctuations, it may be possible to evade long-range magnetic order. For example, the association of spin-chains and spin-ladders in $(La,Y,Sr,Ca)_{14}Cu_{24}O_{41}$ showed superconductivity, associated with the promoted spin gap[22-23] Another conspicuous example is Cu_2OSeO_3 which has a chiral lattice built by inner-Cu_4 tetrahedra and hosts several skyrmion phases.[24]

Here, we show that the compound $Cu_3Te_2O_5(OH)_4$ realizes a novel magnetic topology, so-called "*magnetic raft*" which is built on the superposition of orthogonal FM and AFM spin chains connected by frustrated Cu_4 tetrahedral knots. The FM and AFM chains may stabilize QSLs when perturbating inter-exchanges promote geometrical frustration, which correspond to the situation here. Indeed, no magnetic

ordering occurs down to 1.8 K. The coupled "*raft-like*" low-dimensional subsystems with nontrivial topology provide an unprecedented opportunity to explore the confluence of dimensionality and frustration in engendering exotic magnetism.

2. Experimental section

2.1 Synthesis

Single crystals of $Cu_3Te_2O_5(OH)_4$ were grown using a hydrothermal method as detailed in Supplementary Materials (SM). After grinding crystals, single-phase polycrystalline materials, see Figure S1, was obtained and then used to measure the physical properties.

2.2 Characterization

X-ray diffraction data were collected on a Bruker SMART APEX II diffractometer equipped with a 1K CCD area detector using monochromated Mo Kα radiation (λ = 0.71073 Å) at 293 K. The obtained data were integrated using the program SAINT.[25] The data absorption correction applied was based on the program SADABS.[26] Single-crystal data are found in Table S1 (CCDC deposition number 2206912). The purity of phase was checked by a Bruker D8 Advance diffractometer with monochromatic $CuK\alpha_1$ radiation (λ = 1.54056 Å, 40 kV/40 mA). Qualitative EDX analyses were carried out using a Phenom ProX desktop analyzer. Infrared spectra of the reported materials were recorded using a Varian 670-IR FTIR spectrometer.

The direct current (DC) magnetic susceptibilities of the reported compounds $Cu_3Te_2O_5(OH)_4$ were performed using a superconducting quantum interference device (PPMS) magnetometer. The high-field magnetization of $Cu_3Te_2O_5(OH)_4$ was measured using a home-built vibrating sample magnetometer (VSM) under a WM5 water-cooling resistive magnet at the High Magnetic Field Laboratory, CAS, China. Heat capacity measurements were performed using a commercial physical properties measurement system (PPMS-9, Quantum Design) with the heat capacity option.

Density functional theory (DFT) calculations were performed applying the local density approximation (LDA + U, U = 9 eV for Cu atoms) with the Perdew−Burke−Ernzerhof exchange-correlation potential using the Vienna *ab initio* simulation package

(VASP).[27-31]The magnetic susceptibility and magnetization was evaluated by exact diagonalization (ED) of the Heisenberg spin Hamiltonian with quantum operators, $H = \sum_{(i,j)} J_{i,j}\ \vec{S}_i.\vec{S}_j - g\mu_B \vec{H}\ .\sum_i \vec{S}_i$ using FITMART.[32]

3. Results and discussion

$Cu_3Te_2O_5(OH)_4$ crystallizes in the non-centrosymmetric space group *Cmc*2_1 (No.37), with a 2D crystal structure. Its anionic backbone is composed of *trans*-$Cu2O_3(OH)_2$ square pyramids, $Cu1O(OH)_4$ square pyramids, TeO_3 trigonal pyramid, and TeO_4 polyhedra (Figure 1a). Both Cu^{2+} coordination polyhedra are dominated by four planar ligands with Cu-O bond lengths ranging from 1.919(6) to 1.991(5) Å, and a longer Cu-O bond distance of 2.394(9)- 2.486(7) Å (see SM, Figure S4). The chains are linked by edge-sharing (Cu1) and corner-sharing (Cu2), see Figure 1b, and arranged in three-sandwiched layers by the TeO_n units. Altogether, it creates individual 2D blocks stacked along the *b*-axis, see Figure 1c. It is noteworthy that the interleave space consists of the interaction between Te^{4+} lone pair $4s^2$ doublets and protons, which may be viewed as a Van der Waals gap. From the magnetism perspective, a peculiar 2D lattice emerges from the crossing spin-chains (S=1/2) interconnected by Cu_4 tetrahedra, as shown in Figure 1d. Indeed, given the hierarchy of magnetic exchanges discussed later, such 2D blocks show an analogy with a "*magnetic-raft"* made of cross-linked "*legs*", where the central Cu1- chains are surrounded by Cu2 outer-chains, see Figure 1d. Figure 1e exhibits the projection of this lattice in the (*ab*) plane with the addition of the CuO_4 square planes, which host the dx^2-y^2 magnetic orbitals in strong Jahn-Teller d^9 ions.

When scrutinizing the $[Cu_3O_4(OH)_4]^{6-}$ spin-lattice within a 2D-projection, the blocks bear a resemblance to the $[Mn_3O_6(OH)_2]^{8-}$ blocks found in $K_2Mn_3(VO_4)_2(OH)_2$,[33] in which a triangular lattice of $MnO_4(OH)_2$ octahedra incorporates 1/4th of Mn square-shaped vacancies. This topological evolution of the magnetic lattice is depicted in Scheme S1-S2. Of course, the title-compound incorporates several inequivalent magnetic exchanges, resulting in a structural analogy

rather than a magnetic one. Furthermore, the $[Cu_3O_4(OH)_4]^{6-}$ blocks in $Cu_3Te_2O_5(OH)_4$ are 3D-buckled, resulting in an intermediate character between 1/4th depleted triangular lattice and $M_3V_2O_8$ (M=Co, Ni).[34] At first glance, thus, this *S*=1/2 arrangement forms each column of zigzag honeycomb lattices, which bridges two corner-sharing tetrahedral chains (Figure S5). A magnetic lattice of Cu^{2+} ions in the (0 ~1 0) plane of $Cu_3Te_2O_5(OH)_4$ is illustrated in Figure 1d.

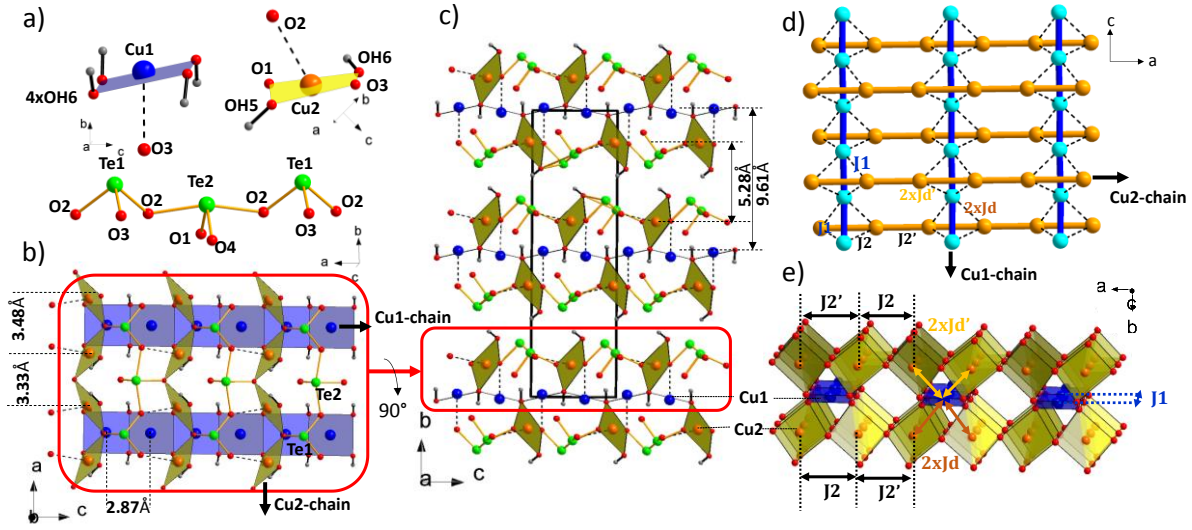

Figure 1. $Cu_3Te_2O_5(OH)_4$ crystal structure: (a) Cu^{2+} and Te^{4+} coordination environments. (b) Arrangement between the Cu1 and the adjacent Cu2 chains projected along the *b*-axis while the low Cu2- sublayer is removed for clarity. (c) Projection along the *a* axis. (d) 2D-spin lattice and dominant magnetic exchanges in the *ac* plane with the "raft" analogy and (e) with evidence of the CuO_4 plaquettes in the (*ab*) plane.

To determine a microscopic magnetic model, we performed spin-polarized DFT+*U* calculations with *U*=9 eV for Cu.[27-31] For simplification, we considered first only the next-neighbors (NN) exchanges along the crossed chains (J_1 and J_2/$J_{2'}$) and a single approximation for interchain exchanges (J_d=$J_{d'}$). The plausible role of further in-chain next-nearest neighbors (NNN) couplings and J_d, $J_{d'}$ differentiation will be discussed later in the frame of our exact diagonalization (ED) fits. After structural relaxation, the total energies for a number of collinear spin configurations onto a classical Heisenberg model have been mapped, see Figure S6. The magnetic model comprising J_1 in the Cu1-chains (or *raft* legs) running along the *c* axis, and J_2, $J_{2'}$

alternating in the Cu2-chains along the *a* axis is shown in Figure 1d,1e. At their intersection, we identified the existence of inter-chain $Cu1_2Cu2_2$ tetrahedral knots containing each 2xJ_d and 2xJ_d'(for $J_{diagonal}$) Cu1-Cu2 exchanges. Here, the fact that Cu1 lies on a mirror symmetry with four J_d, $J_{d'}$ interactions avoids any energy-favorable Cu1 spin arrangement towards Cu2, see Figure S7. The geometrical parameters of the superexchange paths are listed in Table 1.

J_1 is mediated by edge-sharing CuO_4 plaquettes with nearly 90 ° Cu-O-Cu angles. The calculated strong ferromagnetic value of J_1= *-97.6* K is comparable to those of Cu_6 and Cu_{14} spin clusters in the $A_2Cu_3O(CuO)_x(SO_4)_3$ (A = alkali) series, with similar arrangements between CuO_4 plaquettes.[35-36] The other intrachain interactions J_2 (=*147.4* K) and $J_{2'}$ (=*118.4* K) occur through the ~ 120 ° Cu-O-Cu bonds, offering a strong orbital overlap due to the triangular O1(sp^2-like hybridization) and tetrahedral O3 (sp^3-like hybridization) coordinations (see Figure S8). Note that a 2x*a* double-cell was used in order to distinguish J_2 from $J_{2'}$. In the nodal interchain $Cu1_2Cu2_2$ tetrahedra, as mentioned above, we assumed identical J_d and $J_{d'}$ exchanges for the sake of simplicity. We found relatively weak J_d, and $J_{d'}$ interactions of *29.8* K linking the perpendicular legs of our 2D- "raft". Given that each Cu1 ion is coupled to two perpendicular Cu2-chains (above and below) by four Cu1-Cu2 J_d and $J_{d'}$ exchanges, we expect a significant frustration arising from the tetrahedral knots.

Table 1. Magnetic Exchange Geometrical Parameters for Different Exchange Paths in $Cu_3Te_2O_5(OH)_4$. Negative and positive exchange values stand for FM and AFM, respectively. The connection type relies on the CuO_4 coordination, without considering the long Cu-O bonds.

Exchange label and multiplicity / unit cell	Cu-Cu (Å)	Cu-O_{SE} (Å) *O-O	Cu-O-Cu $_{SE}$ (°) ^∠Cu-O-O-Cu (°)	J/K_b (K) DFT+U	J/K_b (K) $_{ED}$ prel./ J_{NNN}
J_1(Cu1-O6-Cu1) 4x edge-sharing	2.87	2x1.96/2x1.97	93.5	*-97.6*	-100/-100
J_{NNN} (Cu1-O6-O6-Cu1)	5.71	* 2x 2.93	^ 51.4	-	- / 50
J_2(Cu2-O1-Cu2) 4x	3.33	2x1.92	120.3	*147.4*	150/148
$J_{2'}$ (Cu2-O3-Cu2) 4x	3.48	2x1.99	121.9	*118.4*	125/125

Corner-sharing					
J_d(Cu1-O6-Cu2) 8x	3.06	1.97/1.94	102.9	*29.8*	51.8/40
$J_{d'}$(Cu2-O6-Cu1) 8x Corner -sharing	3.26	1.94/1.97	113.5	*29.8*	51.8/40

The temperature-dependent magnetic susceptibility $\chi(T)$ of $Cu_3Te_2O_5(OH)_4$ was measured between 2 and 400 K in an applied field of 1000 Oe (see Figure 2a). We observe no bifurcation between the ZFC and FC curves down to 2 K. In the high-temperature region (400-120 K), the Curie-Weiss (CW) fit yields an effective magnetic moment of μ_{eff} = 3.11(1) μ_B per f.u.(formula unit) [= 1.79 μ_B/Cu^{2+})], very close to the S = 1/2 spin-only value (Figure 2a, Figure S9). The CW temperature θ_{CW-1}= -82.3(1) K indicates dominant AFM interactions at high temperatures. The agreement between θ_{CW-1} and the calculated mean-field θ_{CW} of -63.8K[37-39], confirms the significance of our DFT+U calculations and validatethe presence of strong frustration at the intersection of the AF and AFM chains.

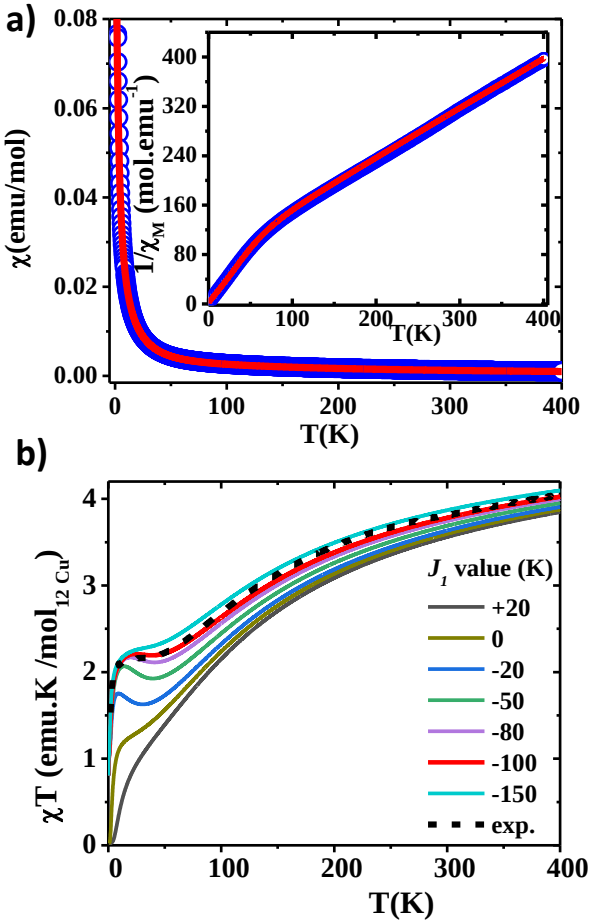

Figure 2. (a) Temperature dependence of the static magnetic susceptibility and $\chi^{-1}(T)$ *vs. T* curve (inset) with ED fitting (red curves) for $Cu_3Te_2O_5(OH)_4$. (b) Experimental χT vs. *T* curve and calculated ones by ED in absence of J_{NNN}, varying J_1 for $J_2/J_{2'}$=148/125 and $J_d=J_{d'}$= 51.8K (see table 1).

Below ~100 K, $\chi^{-1}(T)$ significantly deviates towards a second CW-like regime at low temperatures fitted between 75 K and 2 K with the parameters $\mu_{eff\text{-}2}$ = 2.11(3) μ_B per f.u. and $\theta_{CW\text{-}2}$ = -0.87(6) K, which is close to is the value expected for 1/3rd of paramagnetic Cu^{2+}. As, this low-temperature regime shows a quasi-linear χ^{-1}(T) evolution, its needs careful consideration due its occurrence at the crossover between all exchange couplings, and its very specific frustrated origin. It is a central point of the further discussion below. Notably, the value of $\chi_M T$ is evaluated to be 0.90 emu·mol^{-1}·K at 300 K and decreases gradually with decreasing temperature due to dominant AFM interactions (Figure 2b, S10). On further cooling, a plateau below 50 K and a weak increase at ~25 K point toward the development of short-range FM-like

correlations, which eventually decreases. At 2 K, the $M(H)$ plot displays a nearly-linear increase from −1.5 to 1.5 T and then smoothly increases toward a 1/3rd magnetization plateau at Ms=1.0 μ_B/f.u. as the external field approaches 5 T, which corresponds to two up-spins (↑↑) one down-spin (↓) per f.u. alignment under field (see Figure 3a). This 1/3rd step is stable up to 33T, which is our experimental field limit. The evolution of $M(H)$ at various temperatures is shown in Figure S11.

To validate the "raft" model proposed by DFT+U and figure out the complex magnetic behavior, we used exact diagonalization (ED), for χ(T) and M(H) using the same spin-Hamiltonian . Our preliminary calculations involved twelve S= ½ spins (2^{12} =4096 states) arranged in one AFM ring (J_2, J_2', eight spins) and one FM ring (J_1, four spins) interconnected by J_d with respect the exchange multiplicities, see Figure S12. An excellent match between the experimental and calculated $\chi(T)$ and $\chi T(T)$ was achieved with the values of J_1 =-100 K, $J_2/J_{2'}$ =150 K /125 K, and J_d=51.8 K, see Table 1. It turns out that the J_d value is about ~1.7 times its DFT+U value . This discrepancy is due to fact that the J_d value includes all small exchange interactions neglected in our minimal spin model in absence of NNN interactions within the preliminary model. At least, ED offers the possibility to tune each individual J contributions to the overall magnetic behavior. We found that the sum contribution of AFM Cu2-chains and either paramagnetic Cu1 or FM Cu1-chains was responsible for the $\chi^{-1}(T)$ deviation. Reproducing the $\chi T(T)$ bump requires the aforementioned J_d value, while its fine tuning strongly impacts the fit. In fact, J_d is set so that the interactions on each Cu1 atom nearly compensate ($4J_d + 2J_1 \sim 0$), rendering Cu1 spins to behave nearly paramagnetically. This scenario accounts for the $M(H)$ plateau related to the progressive polarization of Cu1 spins, while Cu2 are engaged in robust AFM correlations in the $J_2/J_{2'}$ chains. Based on our microscopic model, we can estimate a spin gap for isolated alternating Cu2 spin chains as $\Delta \approx (1-\alpha)^{3/4}(1+\alpha)^{1/4}J_2$ where α is the alternation parameter. [40-41] For the title compound, we have $\alpha = J_{2'}/J_2 \sim 0.83$, giving the spin gap $\Delta \approx 45$K (=67.5 T) consistent with the persistent 1/3rd $M(H)$ plateau up to 33 T (our upper experimental limit), see Figure 3a.

Figures 2b highlights the effect of the FM J_1 magnetic exchange on $\chi T(T)$, while keeping the best $J_2/J_{2'}$ =150/125 K and J_d = 51.8 K fixed. Our simulation shows that although the 1/3rd plateau is preserved from decoupled FM legs (J_1=0) to robust FM legs but, only the quasi-free Cu1 scenario can reproduce all our experimental data.

Although, the origin of the magnetization plateau in $Cu_3Te_2O_5(OH)_4$ differs from "standard" Kagomé or triangular antiferromagnets such as $Cu_3V_2O_7(OH)_2$ $2H_2O$,[42] Cs_2CuBr_4,[43] and $YbMgGaO_4$ [44] (the latter being a QSL candidate) formed within a single magnetic sublattice, a strong analogy remains due to the degeneracy lifting of frustrated Cu1 spins in their infinite chains under a magnetic field. A more scrupulous inspection of the low-field $M(H)$ data reveals an S-shaped curvature (inset of Figure S11) around 2T, highlighted by a dM/dH bump, alluding to the presence of AFM next-nearest-neighbor interaction to form FM-AFM spin chains, similarly to the $LiCuSbO_4$ compound.[45] Quantitatively, adding NNN exchanges (α= -0.5J_{NNN}/J_1 = within the FM-Cu1 chains allows reproducing the S-shaped M(H) inflection, see Figure 3b, without significant change on the susceptibility-related features using the same J_1 and $J_2/J_{2'}$ values as for our preliminary (J_{NNN}=0). As such, introducing intrinsic frustration in the FM chains, does not alter the model of frustrated Cu1 at the crossed-knots between the perpendicular raft-legs. Only, J_d has to be lowered to 40 K, more close to its DFT+U value. These ED data prevail and are listed in Table 1. Importantly, the splitting of J_d into J_d and $J_{d'}$ did not improve the ED fits, in agreement with our J_d =$J_{d'}$ approximation. Also, in the Cu2 AFM spin chains, NNN interactions are not favorable, due to its perfectly linear corner-sharing geometry, and J_{NNN} orbital overlaps are exactly included in the J_{NN} paths. In addition, their corner sharing topology involves oxygen atoms out of the d_{x2-y2} magnetic orbitals with very long O-O separations, see Figure S13. The Figures 3c and 3d show the effect of J_1 while the ferromagnetic Cu1-chains are intrinsically frustrated by J_{NNN}, closer to the reality. Similarly to what is stated for our J_{NNN}-free model, it shows how the FM J_1 needs to overcome the combined effects of AFM J_d and J_{NNN} to develop the 1/3rd M(H) plateau and the low-temperature χT (T)

bump. Finally, it is clear that the significant fitted J_{NNN} value of 50 K, still allows for a correct simulation of the χ^{-1}(T) deviation, see Figure3e.

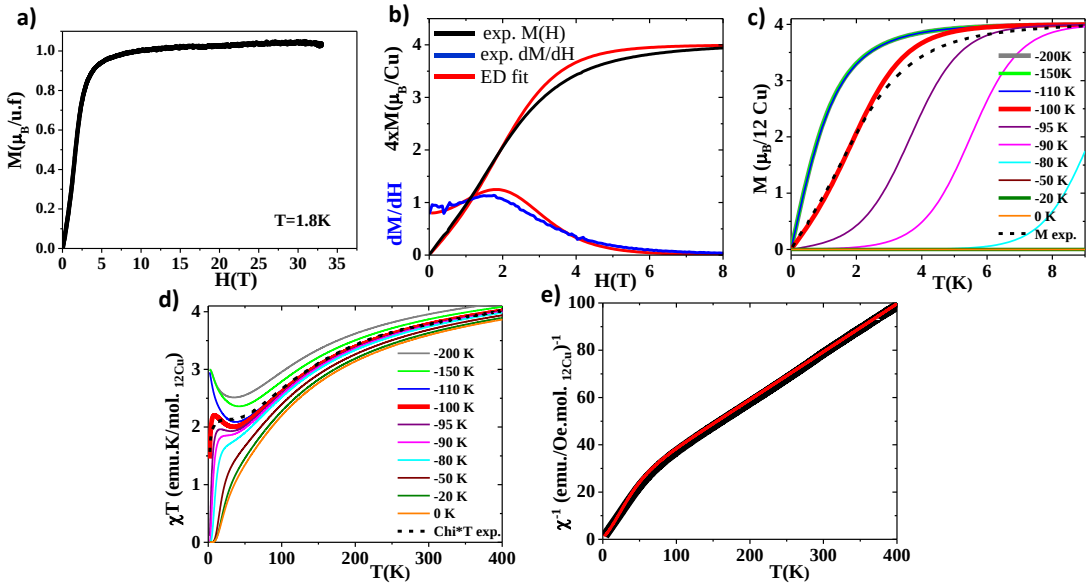

Figure 3. (a) Magnetization vs applied field up to 33 T at T=1.8 K. (b) Influence of AFM J_{NNN} (α= -0.5) on the low-field magnetization, with a correct simulation of the inflection at 2T using J_1= -100 K, J_2=148 K, $J_{2'}$=125 K, J_d=$J_{d'}$=40 K, J_{NNN}=50 K. (c) Isotherm magnetization at 2K and ED simulated ones by ED simulations versus J_1 values using Js of (b). (d) χT(T) ED simulations using same parameters. (e) χ^{-1}(T) ED simulation (red) *vs.* experimental data (black) using the parameters of (b). For (b,c,d,e) J_{NNN} is considered.

We next turn to heat capacity measurements, a highly sensitive probe for low-energy excitations to elucidate the behavior of our "*magnetic-raft*" model in the entire temperature range. The temperature dependence of the specific heat $C_p(T)$ is shown in Figure 4a. We observe no λ-like peak down to 1.8 K, excluding the development of long-range magnetic ordering with measured temperature window and raising the possibility of QSLs. Above 100 K, $C_p(T)$ was fitted as a sum of Debye and Einstein functions to extract the lattice contribution:

$$C_{\mathrm{lat}}(T) = 9C_{\mathrm{D}}Nk_{\mathrm{B}}\left(\frac{T}{\theta_{\mathrm{D}}}\right)^3 \int_0^{\theta_{\mathrm{D}}/T} \frac{x^4 e^x}{(e^x-1)^2}\,dx + 3Nk_{\mathrm{B}}C_{\mathrm{E}}\left(\frac{\theta_{\mathrm{E}}}{T}\right)^2 \frac{e^{\theta_E/T}}{(e^{\theta_E/T}-1)^2}.$$

Here, C_D (C_E) is the weighting factor for the Debye (Einstein) term, k_B is the Boltzmann constant, and θ_D (θ_E) is the Debye (Einstein) temperature. The sum of the weighting factors was fixed to match the total number of atoms (per f.u.) divided by the number

of Cu ions (C_D+C_E=18/3=6). This yields C_D=3.2(3), θ_D=331(7) K, C_E=2.8(3), and θ_E=1028(17) K, see Figure 4a.

Assuming no electronic contribution, $C_m(T)$ can be obtained by subtracting $C_{lat}(T)$ from $C_p(T)$. On cooling below 75 K, $C_m(T)$ increases gradually and shows a broad maximum at 40 K. The onset temperature of $C_m(T)$ is comparable to $|\theta_{CW1}|$=82.3 K, marking the gradual development of spin correlations. As the temperature is lowered, $C_m(T)/T$ exhibits a broad maximum at T_{max}=31 K, and then a subsequent decrease down to 10 K, and finally an abrupt upturn, see Figure 4b. The broad maximum in $C_m(T)/T$ is characteristic of gapped excitations in low-dimensional magnets, and primarily attributed to the alternating Cu2 AFM chains. Notably, the spin gap $\Delta \approx 45$ K estimated above is comparable to the energy scale of T_{max}=31 K.

Below this peak, the upturning feature of $C_m(T)/T$ follows a power law of $C_m(T)/T \sim T^{-1.84(1)}$ below 7 K, heralding the presence of a large density of magnetic states (see Figure S14). In Figure 4c, the temperature dependence of the specific heat at different fields apparently shows an upturning feature at low T. Considering its field evolution, we infer the presence of weakly correlated orphan or magnetic impurities showing the Schottky anomaly. The Schottky contribution is given by $C_{\mathrm{Sch}} = NR\left(\frac{\Delta}{k_B T}\right)^2 e^{\Delta/k_B T} / \left[1 + e^{\Delta/k_B T}\right]^2$, where N= 0.136(6) is the fraction of weakly coupled spins, consistent with 14 % of weakly coupled spins estimated from the magnetic entropy mentioned below. R is the ideal gas constant, and Δ is the Schottky gap. In the inset of Figure 4c, we plot the field dependence of the extracted Schottky energy level. $\Delta/k_B(B)$ exhibits a linear increment with increasing field. The linear relation $\Delta(B) = \Delta_0 + g\mu_B B$ is well known for electronic Schottky anomaly by orphan or magnetic impurities. From the fittings, we obtain the zero-field Schottky gap of Δ_0/k_B=1.9(4) K and the g-factor of 2.89(8). The larger g-factor than the Cu^{2+} value in octahedral crystal fields ($g_{Cu^{2+}} \approx 2.1$-2.5) [46] implies that the orphan or magnetic impurities are dressed by other exchange couplings at low temperatures.

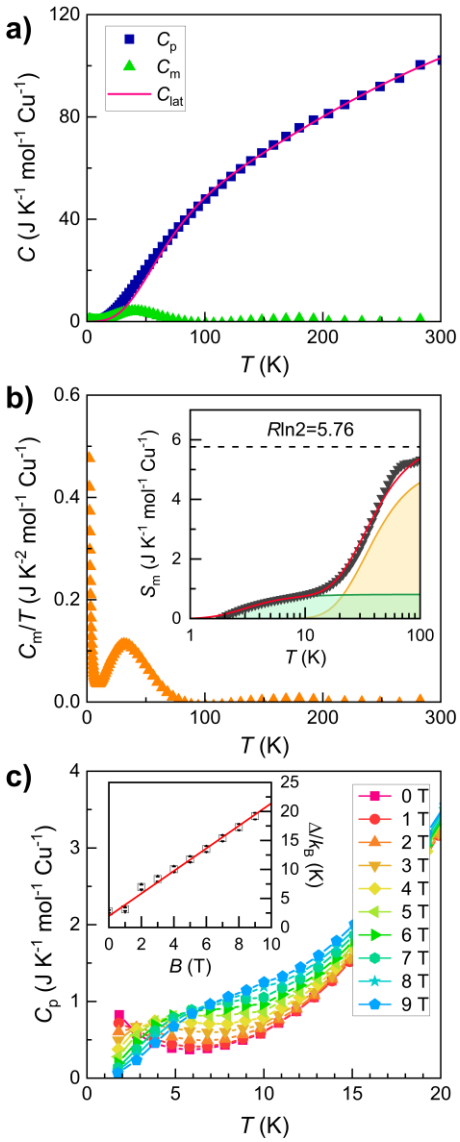

Figure 4 (a) Temperature dependence of the total specific heat $C_p(T)$ plotted together with the lattice contribution $C_{lat}(T)$ (pink solid line) and the magnetic specific heat $C_m(T)$ (green triangles). (b) Magnetic specific heat divided by temperature as a function of temperature $C_m(T)/T$. The inset displays a calculated magnetic entropy $S_m(T)$ obtained by integrating $C_m(T)/T$. $S_m(T)$ can be decomposed into two Schottky entropy terms, depicted as shadings. (c) Temperature dependence of Cp/T under different magnetic fields. The inset shows the spin gap Δ extracted from the Schottky anomaly.

Quantitatively, the magnetic entropy $S_m(T)$ is deduced by the integration of $C_m(T)/T$, as shown in the inset of Figure 4b. $S_m(T)$ saturates to the value of 5.336 J K^{-2} mol^{-1} Cu^{-1} at 100 K, which is about 92% of the theoretically expected value Rln(2S+1)=5.76 J K^{-}

^{2} mol^{-1} Cu^{-1} for S=1/2. $S_m(T)$ confirms a two-step release of the magnetic entropy in the two different temperature ranges, T=1.8-15 K and 20-100 K, which is well reproduced by two Schottky entropy functions,

$$S_{\mathrm{m}}(T) = \sum_{i=1,2} a_i \left[\ln\left(1 + e^{T_i/T}\right) - \frac{T_i}{T} \frac{e^{T_i/T}}{1 + e^{T_i/T}} \right],$$

where a_i is the weighting factor, and T_i is the characteristic temperature for the entropy release. We obtain the fitting parameters of a_1=1.16(5) J K^{-2} mol^{-1} Cu^{-1}, T_1=7.1(5) K, a_2=7.38(6) J K^{-2} mol^{-1} Cu^{-1}, and T_2=80(1) K. Each component is marked in the inset of Figure 4b as the color shadings. The low-T and high-T components saturate to 0.808 J K^{-2} mol^{-1} Cu^{-1} and 5.118 J K^{-2} mol^{-1} Cu^{-1}, which correspond to 14% and 86% of the released total magnetic entropy, respectively. This suggests that the Cu1 spins release their magnetic entropy in two steps: first, a part of $S_m(T)$ is released in their frustrated tetrahedra, and then the remaining $S_m(T)$ is involved in the formation of a spin-dimer-like state at high temperatures. The released magnetic entropy does not follow the ideal 1/3rd (Cu1): 2/3rd (Cu2) ratio, indicative of the presence of pronounced quantum fluctuations of Cu1 spins due to the frustrated tetrahedral couplings.

The released 8% missing entropy is assigned to residual low-T fluctuations below 2 K, in agreement with the inferred liquid-state. The intertwining between the alternating Cu2 chains and the FM Cu1 chains results in an in-gap state, causing a spin dimer to evolve into a quantum paramagnetic state. This is inferred from the steep low-T upturn that is reminiscent of a paramagnetic Schottky anomaly. Admittedly, dilution specific heat data may help identify the true ground state, but it is beyond the scope of this study. However, it is of primal importance to recall how different the ratio of magnetic entropy present at low temperature can be depending on the spin-liquid "*flavor*" . For instance in $LiCuSbO_4$ [45] with suggested QSL hold by FM-AFM$_{(NNN)}$ chains, thermodynamic measurements at 0 T validates a quasi total release of the entropy at 50 K, while in contrast, the QSL in $Na_2BaCo(PO_4)_2$ [47] exhibits low-energy spin fluctuations that preserve ~ 30% of the magnetic entropy below 1K. Our 8%

amount suggests a moderate degree of spin fluctuation, but concentrated essentially on 1/3rd of the Cu ions, i.e. Cu1.

Finally, our system shows similarities in magnetic ingredients and behaviors to CuP_2O_6.[48] In this compound, the coupling between strongly coupled 2D subunits is frustrated by weakly-coupled sandwiched 1D subunits, which reduces significantly the expected ordering temperature. Similarly, in $Cu_3Te_2O_5(OH)_4$, the 3D ordering should involve both the Cu1 and Cu2 1D-sublattices, as interactions between Cu2 atoms occur via Cu1 and vice-versa. The inclusion of J_d leads to almost perfect frustration on Cu1, while promoting quantum fluctuations. Dilfridge temperature measurements are needed to differentiate whether the title compound harbors the true QSL or not.

4. Conclusions

To conclude, we have combined density functional calculations and ED simulations with magnetic susceptibility, high-field magnetization, and specific heat measurements to deduce a spin lattice of $Cu_3Te_2O_5(OH)_4$. We find that $Cu_3Te_2O_5(OH)_4$ comprises two distinct sublattices: FM and alternating AFM S= ½ chains interconnected by frustrated knots. The participation of significant NNN interactions in the ferromagnetic sub-units was deduced from ED simulations of M(H) data, but does not fundamentally change the magnetic behavior of this complex system. Indeed, collectively, they form a so-called 2D "*magnetic raft*", which is a promising host of QSL. Frustration involved plays a vital role in the low-energy physics of this exotic system, decoupling two subsystems as manifested in a two-stage release of magnetic entropy with temperature, a two Curie-Weiss regime of the magnetic susceptibility, and a 1/3rd magnetization plateau stable up 33 T. At high temperatures and magnetic fields, spin-dimer correlations govern spin dynamics. On the other hand, the low-temperature and field physics is dictated by frustrated interchain knots of the two heterogenous subchains. Unlike coupled homogeneous spin chains, quantum fluctuations amplified by frustrated tetrahedral interconnection of the two spin chains prevent the development of 3D magnetic ordering. As such, the title compound opens up a new avenue to achieve

a quantum spin liquid or a quantum paramagnet when the two orthogonally arranged heterogeneous spin chains are coupled by frustrated interactions.

AUTHOR INFORMATION

 # Corresponding Author

E-mail address:

m.f.lv@hotmail.com (Minfeng Lü)

olivier.mentre@univ-lille.fr (Olivier Mentré)

ORCID[ID]

Minfeng Lü: 0000-0003-2576-3840

Angel M. Arévalo-López: 0000-0002-8745-4990

Notes

The authors declare no competing financial interests.

Acknowledgments

This work was financially supported by the National Natural Science Foundation of China (21671185). C^{2}TN/IST authors gratefully acknowledge the FCT support through the UID/Multi/04349/2013 project. The work at SKKU was supported by the National Research Foundation (NRF) of Korea (Grant no. 2020R1A5A1016518). OM, AAL and CM thank support from ANR AMANTS project (19-CE08-0002-01) and the Chevreul Institute (FR 2638), Region Hauts-de-France, and FEDER are acknowledged for funding the PPMS equipment.

References:

(1) Urano, C.; Nohara, M.; Kondo, S.; Sakai, F.; Takagi, H.;Shiraki, T.; Okubo, T. LiV_2O_4 spinel as a heavy-mass Fermi liquid:Anomalous transport and role of geometrical frustration. *Phys. Rev.Lett.* **2000**, *85*, 1052.

(2) Balents, L. Condensed-Matter Physics: Quantum Mechanics in a Spin. *Nature* **2016**, *540*, 534−535.

(3) Bramwell, S. T.; Giblin, S. R.; Calder, S.; Aldus, R.; Prabhakaran, D.; Fennell, T. Measurement of the charge and current of magnetic monopoles in spin ice. *Nature* **2009**, *461*, 956−959.

(4) Anderson, P. W. *RVB Theory of High Tc Superconductivity. In Novel Superconductivity*; Springer, Boston, MA, 1987; pp 295−299.

(5) Lee, P. A. From High Temperature Superconductivity to Quantum Spin Liquid: Progress in Strong Correlation Physics. *Rep.Prog. Phys.* **2008**, *71*, 012501.
(6) Zhang, L.; Ren, J.; Wang, J.-S.; Li, B. Topological Magnon Insulator in Insulating Ferromagnet. *Phys. Rev. B* **2013**, *87*, 144101.
(7) Chisnell, R.; Helton, J. S.; Freedman, D. E.; Singh, D. K.; Bewley, R. I.; Nocera, D. G.; Lee, Y. S. Topological Magnon Bands in a Kagomé Lattice Ferromagnet. *Phys. Rev. Lett.* **2015**, *115*, 147201.
(8) Wang, C.; Nahum, A.; Senthil, T. Topological Paramagnetism in Frustrated Spin-1 Mott Insulators. *Phys. Rev. B* **2015**, *91*, 195131.
(9) Mermin, N. D.; Wagner, H. Absence of ferromagnetism or antiferromagnetism in one-or two-dimensional isotropic Heisenberg models.*Phys. Rev. Lett.* **1966**, *17*, 1133.
(10) Scalapino, D. J.; Imry, Y.; Pincus, P. Generalized Ginzburg-Landau theory of pseudo-one-dimensional systems. *Phys. Rev. B* **1975**, *11*, 2042.
(11) Schulz, H. J. Dynamics of coupled quantum spin chains.*Phys. Rev. Lett.* **1996**, *77*, 2790.
(12) Aidoudi, F. H.; Aldous, D. W.; Goff, R. J.; SlawinAlexandra, M. Z.; Attfield, J. P.; Morris, R. E.; Lightfoot, P. An ionothermally prepared S= 1/2 vanadium oxyfluoride Kagomé lattice.*Nat. Chem.* **2011**, *3*, 801-806.
(13) Shores, M. P. ; Nytko, E. A. ; Bartlett, B. M.; Nocera, D. G. A Structurally Perfect S = 1/2 Kagomé Antiferromagnet. *J. Am. Chem. Soc.* **2005**, *127*, 13462-13463.
(14) II, M.S.; Wang, X.; Koo, H.-J.; Whangbo, M-H.; Jacobson, A. J. Synthesis of the Elusive S = ½ Star Structure:A Possible Quantum Spin Liquid Candidate. *J. Am. Chem. Soc.* **2020**, *142*, 5013–5016.
(15)Winiarski, M. J.; Tran, T. T.; Chamorro, J. R.; McQueen,T. M. (Cs*X*)$Cu_5O_2(PO_4)_2$ (*X* = Cl, Br, I): A Family of Cu^{2+} $S = {}^1/_2$ Compounds with Capped-Kagomé Networks Composed of OCu_4 Units.*Inorg. Chem.* **2019**, **58**, 4328–4336.
(16) W.-B. Guo, Y.-Y. Tang, J. Wang, Z. He, Layered $Cu_7(TeO_3)_2(SO_4)_2(OH)_6$ with Diluted Kagomé Net Containing Frustrated Corner-Sharing Triangles. *Inorg. Chem.* **2017**, *56*, 1830–1834.
(17) Baenitz, M.; Geibel, C.; Dischner, M.; Sparn, G.; Steglich, F.;Otto, H. H.; Meibohm, M.; Gippius, A. A. $CuSiO_3$: A quasi-onedimensional S = 1/2 antiferromagnetic chain system. *Phys. Rev. B* **2000**, *62*, 12201.
(18) Tsukada, I.; Sasago, Y.; Uchinokura, K.; Zheludev, A.; Maslov,S.; Shirane, G.; Kakurai, K.; Ressouche, E. $BaCu_2Si_2O_7$: A quasi-onedimensional S = 1/2 antiferromagnetic chain system. *Phys. Rev. B* **1999**, *60*, 6601.
(19) Tsukada, I.; Takeya, J.; Masuda, T.; Uchinokura, K. Weak ferromagnetism of quasi-one-dimensional S = 1/2 antiferromagnet $BaCu_2Ge_2O_7$. *Phys. Rev. B* **2000**, *62*, R6061−6064.
(20) Hase, M.; Terasaki, I.; Uchinokura, K. Observation of the spin-Peierls transition in linear Cu^{2+} (spin-1/2) chains in an inorganic compound $CuGeO_3$. *Phys. Rev. Lett.* **1993**, *70*, 3651.
(21) Gautier, R.; Oka, K.; Kihara, T.; Kumar, N.; Sundaresan, A. ;Tokunaga, M. ; Azuma, M. ; Poeppelmeier, K. R.Spin Frustration from cis-Edge or -Corner Sharing Metal-Centered Octahedra. *J. Am. Chem. Soc.* **2013**, *135*, 19268-19274.
(22)Vuletić, T.; Korin-Hamzić, B.; Ivek,T.; Tomić,S.; Gorshunov,B.; Dressel,M.; Akimitsu, J. The spin-ladder and spin-chain system $(La,Y,Sr,Ca)_{14}Cu_{24}O_{41}$: Electronic phases, charge and spin dynamics. *Phys.Rep*. **2006**, *428*, 169 – 258.
(23)Lemmens, P.; Güntherodt, G.; Gros, C.Magnetic light scattering in low-dimensional quantum spin systems. *Phys.Rep*. **2003**,*376*,1-103.
(24)Chacon, A.; Heinen, L.; Halder, M.; Bauer, A.; Simeth, W.; Mühlbauer, S.; Berger, H.; Garst, M.; Rosch, A.; Pfleiderer, C. Observation of two independent skyrmion phases in a chiral magnetic material, Nat. Phys. **2018**, *14*, 936.

(25) SAINT: Area-Detector Integration Software; Siemens Industrial Automation, Inc.: Madison, 1996.
(26) SADABS: Area-Detector Absorption Correction; Siemens Industrial Automation, Inc.: Madison, 1995.
(27) Koepernik,K.; Eschrig, H. Full-potential nonorthogonal local-orbital minimum-basis band-structure scheme. *Phys. Rev. B* **1999**, *59*, 1743.
(28) Perdew, J. P.; Wang, Y. Pair-distribution function and its coupling-constant average for the spin-polarized electron gas. *Phys. Rev. B* **1992**, *45*, 13244.
(29) Kresse, G.; Furthmüller, J. *Vienna Ab-initio Simulation Package (VASP)*; Institut für Materialphysik: Vienna, Austria, 2004.
(30) Kresse, G.; Furthmüller,J. Efficiency of ab-initio total energy calculations for metals and semiconductors using a plane-wave basis set. *Comput. Mater. Sci.* **1996**, *6*, 15;
(31) Kresse, G.; Furthmüller, J.Efficient iterative schemes for ab initio total-energy calculations using a plane-wave basis set. *Phys. Rev. B* **1996**, *54*, 11169.
(32) Engelhardt, L.; Garland, S. C.; Rainey, C.; Freeman, R. A. FIT-MART: quantum magnetism with a gentle learning curve. *Physics Procedia* **2014**, *53*, 39– 43.
(33) Liao, H.; Guyomard, D.; Piffard, Y.; Tournoux, M. $K_2Mn_3(OH)_2(VO_4)_2$, a New Two- Dimensional Potassium Manganese(II) Hydroxyvanadate. *Acta Cryst.* **1996** ,*C52*, 284-286.
(34) Lawes, G.; Kenzelmann, M.; Rogado, N.; Kim, K. H.; Jorge, G. A.; Cava, R. J.; Aharony, A.; Entin-Wohlman, O.; Harris, A. B.; Yildirim, T.; Huang, Q. Z.; Park, S.; Broholm, C. ; Ramirez, A. P. Competing Magnetic Phases on a Kagomé Staircase. *Phys. Rev. Lett.* **2004**, *93*,247201.
(35) Nekrasova, D.O.; Tsirlin, A.A.; Colmont, M.; Siidra, O.; Vezin, H.; Mentré, O.Magnetic hexamers interacting in layers in the $(Na,K)_2Cu_3O(SO_4)_3$ minerals. *Phys. Rev. B* **2020**, *102*, 184405.
(36) Nekrasova, D.O.; Tsirlin, A. A.; Colmont, M.; Siidra, O. I. ; Arévalo-López, Á.M.; Mentré,O. From (S = 1) Spin Hexamer to Spin Tetradecamer by CuO Interstitials in $A_2Cu_3O(CuO)_x(SO_4)_3$ (A = alkali). *Inorg. Chem.* **2021**, *60*, 18185–18191.
(37) *Mean Field* : $\theta_{CW} = S(S+1)^* [1_{Cu1}x(2J_1+4J_d) + 2_{Cu2}x(J_2+J_{2'}+2J_d)]/(3_{Cu}x3) = -63.8K$
(38) Kahn,O. *Molecular Magnetism*. Wiley VCH 1993; P.26-29.
(39) Lee,K.H.; Lee,J.Y.; Lee,C.; Whangbo,M.-H. Evaluating the Curie-Weiss Temperature of a Magnetic System Composed of Nonequivalent Magnetic Ions in Terms of Spin Exchange Constants.*Bull. Korean Chem. Soc.* **2014**, *35*, 1277.
(40) Barnes,T.; Riera, J.; Tennant, D. A. S=1/2 alternating chain using multiprecision methods.*Phys. Rev. B* **1999**, *59*, 11384.
(41) Johnston, D. C.; Kremer, R. K.; Troyer,M.; Wang, X.; Klümper, A.; Budko, S. L.; Panchula, F.; Canfield, P. C. Thermodynamics of spin antiferromagnetic uniform and alternating-exchange Heisenberg chains. *Phys. Rev. B* **2000**, *61*, 9558.
(42) Ishikawa, H.; Yoshida, M.; Nawa, K.; Jeong, M.; Krämer, S.; Horvatić, M.; Berthier, C.; Takigawa, M.; Akaki, M.; Miyake, A.; Tokunaga, M.; Kindo, K.; Yamaura, J.; Okamoto,Y.; Hiroi, Z. One-third magnetization plateau with a preceding novel phase in volborthite.*Phys. Rev. Lett.* **2015**, *114*, 227202.
(43) Fortune, N. A.; Hannahs, S. T.; Yoshida,Y.; Sherline,T. E.; Ono,T.; Tanaka, H.; Takano,Y.Cascade of Magnetic-Field-Induced Quantum Phase Transitions in a Spin-1/2 Triangular-Lattice Antiferromagnet.*Phys. Rev. Lett.* **2009**, *102*, 257201.
(44) Li,Y.; Liao, H.; Zhang, Z.; Li, S.; Jin, F.; Ling, L.; Zhang, L.; Zou, Y.; Pi, L.; Yang, Z.; Wang, J.; Wu, Z.; Zhang,Q. Gapless quantum spin liquid ground state in the two-dimensional spin-1/2 triangular antiferromagnet $YbMgGaO_4$.*Sci. Rep.* **2015**, *5*, 16419.

(45) Dutton, S. E.; Kumar, M.; Mourigal, M.; Soos, Z. G.; Wen, J.-J.; Broholm, C. L.; Andersen, N. H.; Huang,Q.; Zbiri, M.; Toft-Petersen, R.; Cava,R. J. Quantum Spin Liquid in Frustrated One-Dimensional $LiCuSbO_4$. *Phys. Rev. Lett.* **2012**,*108*, 187206.

(46) Dang,L.S.; Buisson, R.; Williams, F.I.B. Dynamics of an octahedral Cu^{2+} jahn-teller system. consequences on its electron spin resonance.J. Phys. France,1974, **35**, 49-65.

(47) Zhong,R.;Guo,S.;Xu,G.;Cava, R. J. Strong quantum fluctuations in a quantum spin liquid candidate with a Co-based triangular lattice. *PNAS* **2019**,*116*,14505-14510.

(48) Nath, R.; Ranjith, K.M.; Sichelschmidt, J.; Baenitz, M.; Skourski,Y.; Alet, F.; Rousochatzakis, I.; Tsirlin, A. A. Hindered magnetic order from mixed dimensionalities in CuP_2O_6.*Phys. Rev. B* **2014**, *89*, 014407.

TOC graphic